JOURNAL OF GEOPHYSICAL RESEARCH, VOL. 114, A05218, doi:10.1029/2009JA014069, 2009

Electron densities in Jupiter's outer magnetosphere determined from Voyager 1 and 2 plasma wave spectra

B. L. Barnhart,[1] W. S. Kurth,[1] J. B. Groene,[1] J. B. Faden,[1] O. Santolik,[2] and D. A. Gurnett[1]

Received 16 January 2009; revised 19 March 2009; accepted 23 March 2009; published 27 May 2009.

[1] This paper presents an electron plasma density data set for Jupiter's outer magnetosphere derived from high-resolution wideband measurements of low-frequency radio and plasma waves obtained by Voyagers 1 and 2 during their 1979 flybys. This work utilizes a new data processing tool that makes important improvements in the identification of the plasma frequency and other characteristic frequencies of the plasma, thereby allowing for the determination of the electron density within the Jovian magnetosphere. Furthermore, this work includes the interpretation of complex spectra including sometimes overlapping wave phenomena including continuum radiation, Z mode emissions, and whistler mode waves. Using the theory of cold plasmas and measurements of the magnetic field from which the electron cyclotron frequency can be calculated, we establish an extensive set of reasoning for interpreting cutoffs and resonances in the wave spectra to identify characteristic frequencies of the plasma, including the electron plasma frequency, $R = 0$ cutoff, $L = 0$ cutoff, and upper hybrid resonance frequency. While most Voyager plasma wave data used are obtained in the plasma sheet where the plasma frequency is greater than the cyclotron frequency, this investigation also analyzes observations in the lobe where the cyclotron frequency is greater than the plasma frequency to interpret the various cutoffs and resonances in the spectrum. The resulting data set for the electron densities has higher temporal resolution than any others that exist today. Also, given the identification of spectral features to accuracies of $\sim$100 Hz or better, the density measurements are among the most accurate for Jupiter's magnetosphere.

Citation: Barnhart, B. L., W. S. Kurth, J. B. Groene, J. B. Faden, O. Santolik, and D. A. Gurnett (2009), Electron densities in Jupiter's outer magnetosphere determined from Voyager 1 and 2 plasma wave spectra, *J. Geophys. Res.*, *114*, A05218, doi:10.1029/2009JA014069.

1. Introduction

[2] Nonthermal continuum radiation is prevalent in the outer regions of both the terrestrial and Jovian magnetospheres. Data from the Imp 6 and Imp 8 missions were used to demonstrate that this electromagnetic radiation propagates in the ordinary mode above a lower cutoff frequency at the local electron plasma frequency [*Gurnett and Shaw*, 1973; *Gurnett*, 1975]. Similar electromagnetic radiation was first discovered at Jupiter using the Voyager Plasma Wave Receiver [*Scarf et al.*, 1979; *Gurnett et al.*, 1979]. These emissions have been used to infer the plasma density in the Jovian magnetosphere [*Scarf et al.*, 1979; *Gurnett et al.*, 1979; *Barbosa et al.*, 1990; *Gurnett et al.*, 1980]. However, the only attempt to systematically determine the plasma density using high resolution wideband waveform data was by *Ansher et al.* [1992].

[3] The nonthermal continuum radiation found at Jupiter spans frequencies higher and lower than the solar wind plasma frequency. Emissions at frequencies greater than the solar wind plasma frequency propagate freely out of the magnetosphere while the lower frequencies are trapped between the higher frequency boundaries of the magnetopause and the dense inner regions of the magnetosphere [*Gurnett et al.*, 1980, 1981].

[4] The trapped continuum radiation exhibits a lower cutoff, below which no waves propagate [*Gurnett and Shaw*, 1973; *Stix*, 1962]. This cutoff is the electron plasma frequency (f_{pe}), which is related to the local electron plasma density by the relation

$$f_{pe} = 8980\sqrt{n_e}, \quad (1)$$

where f_{pe} is in Hz and the electron density n_e is in cm^{-3} [*Stix*, 1962]. The plasma frequency is just one of several characteristic frequencies defined in cold plasma theory. Others are the electron cyclotron frequency f_{ce}, the right and left hand cutoffs $f_{R=0}$ and $f_{L=0}$, and the upper hybrid

[1] Department of Physics and Astronomy, University of Iowa, Iowa City, Iowa, USA.
[2] Faculty of Mathematics and Physics, Charles University, Prague, Czech Republic.

0148-0227/09/2009JA014069$09.00

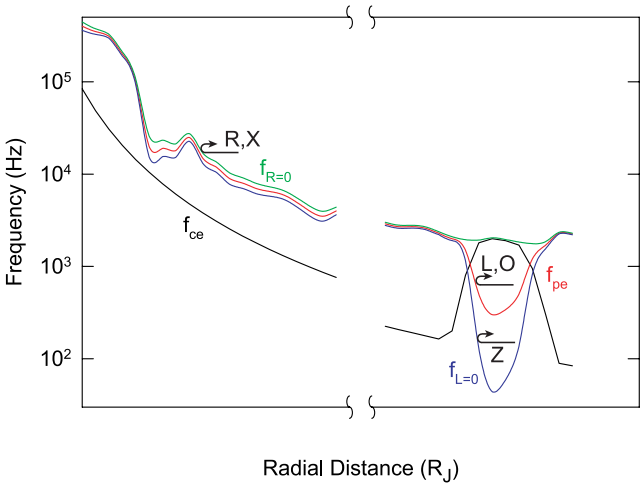

Figure 1. Sketch of the characteristic frequencies found in the Jovian magnetosphere. Two separate regions are displayed, wherein $f_{pe} > f_{ce}$ and $f_{pe} \ll f_{ce}$. The sketch illustrates the relationships between the various cutoffs and is designed to show, qualitatively, the variations between the various characteristic frequencies in different regions of the magnetosphere. Examples of actual spectra are given in later sections.

resonance frequency f_{UH}. These frequencies are related to one another by the following formulas:

$$f_{ce} = 28|B| \tag{2}$$

$$f_{R=0} = \frac{f_{ce}}{2} + \sqrt{(f_{pe})^2 + \left(\frac{f_{ce}}{2}\right)^2} \tag{3}$$

$$f_{L=0} = -\frac{f_{ce}}{2} + \sqrt{(f_{pe})^2 + \left(\frac{f_{ce}}{2}\right)^2} \tag{4}$$

$$f_{UH}^2 = f_{pe}^2 + f_{ce}^2. \tag{5}$$

In equation (2), $|B|$ is the magnitude of the magnetic field in nT and the units of all frequencies are in Hz. The cyclotron frequency can be accurately determined from magnetometer measurements making f_{ce} known almost everywhere wideband data exist.

[5] Figure 1 is a sketch of the characteristic frequencies of the plasma as a function of distance from Jupiter. The distance axis is not to scale, but is designed to show the situation in the plasma sheet where the electron plasma frequency f_{pe} is greater than f_{ce} and another region, representative of the lobe of the magnetosphere, where f_{ce} is greater than f_{pe}.

[6] Figure 2, after *Gurnett and Bhattacharjee* [2005], illustrates four distinct wave modes which are designated by the waves' polarization and electric field component's orientation with respect to the local magnetic field. Conventionally, the polarization is labeled as either L for left-handed polarization or R for right-handed polarization. Also, the orientation of the electric field component is

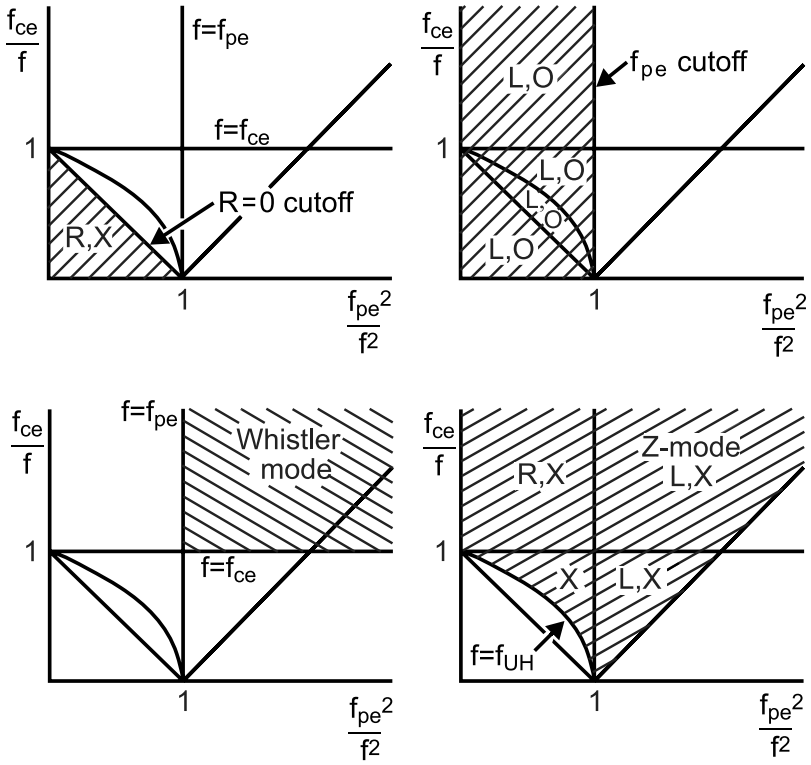

Figure 2. Clemmow-Mullaly-Allis (CMA) diagrams after *Gurnett and Bhattacharjee* [2005] illustrating the theoretically allowed propagation of various wave modes. Also, the characteristic frequencies of these modes (representing cutoffs or resonances) are displayed. The frequencies are defined in equations (1)–(5), and f is the frequency of the wave.

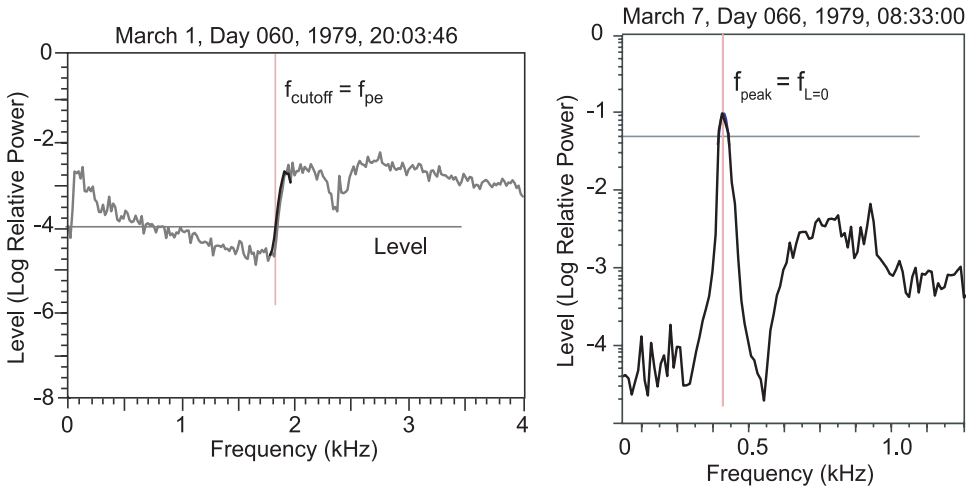

Figure 3. Examples displaying results from the new cutoff and peak detection tools. (left) f_{pe} measured from the sharp cutoff of the power spectrum at approximately 1.8 kHz. (right) Detection of a peak in the spectrum interpreted as $f_{L=0}$.

labeled either O for ordinary, meaning parallel to the local magnetic field or X for extraordinary, meaning perpendicular to the local magnetic field. Thus we have four modes possible: the left-handed ordinary mode (L, O), the left-handed extraordinary mode (L, X) otherwise known as the Z mode, the right-handed extraordinary mode (R, X), and the whistler mode.

[7] Each mode propagates within a certain frequency range, as displayed in Figure 2, and exhibits a cutoff where its index of refraction goes to zero, and some can experience resonances such as the upper hybrid resonance, as in equation (5).

[8] In the simplest spectra when $f_{pe} \gg f_{ce}$ in the plasma sheet, only the nonthermal continuum radiation needs to be considered and we interpret the low-frequency cutoff of this emission as the electron plasma frequency as previously assumed by *Shaw and Gurnett* [1980], *Moses et al.* [1987], and *Barbosa et al.* [1990]. Strictly speaking, this cutoff is an upper limit to the local electron plasma frequency due to the potential of a high density region existing between the radio emission source and the spacecraft. When this occurs, the cutoff measurement pertains to the distant density structure rather than the local cutoff. However, the cutoffs measured are usually sharp which suggests a local cutoff [*Gurnett et al.*, 1981]. In a more complex spectrum within the plasma sheet consisting of a mix of both ordinary and extraordinary modes, the continuum radiation may exhibit a partial cutoff at a somewhat higher frequency than the plasma frequency, which can be interpreted as the cutoff of the extraordinary mode at $f_{R=0}$. In other complex cases, Z mode radiation is observed at lower frequencies [*Kennel et al.*, 1987; *Barbosa et al.*, 1990]; the low-frequency cutoff of this emission is at $f_{L=0}$. Occasionally, an enhancement is seen near the low-frequency cutoff of the continuum radiation and corresponds to the upper hybrid resonance frequency f_{UH}. Given the relations above, it is clear that if one of these characteristic frequencies can be identified (in addition to f_{ce}), one can determine f_{pe} and an estimate of the electron density can be made. In the lobes, when $f_{pe} \ll f_{ce}$, there is a mixture of modes (ordinary, Z mode, whistler) which exhibit one or more cutoffs within the spectrum. *Perraut et al.* [1998] encountered similar examples using Galileo data. Using the relations above, we will calculate the various frequencies, and therefore densities, for similar regions and compare our results with those found by *Perraut et al.* [1998].

[9] We will discuss a new electron density data set generated using a new, semiautomated analysis tool. The data set represents the highest resolution measurements of the electron density at Jupiter. We will also comment on the accuracy and limitations of the density measurements. We will discuss the methods and criteria used in selecting the various characteristic frequencies. In many instances, two or more of the characteristic frequencies can be identified at a given time. This provides an opportunity to check for consistency between the multiple identifications to both validate the interpretation of the characteristic frequencies, and to assess the accuracy of the density determination.

[10] For a full description of the Voyager 1 and 2 plasma wave instrumentation, see *Scarf and Gurnett* [1977].

2. New Analysis Tools

[11] Previous attempts to derive electron densities from the Voyager wideband data were carried out one spectrum at a time with a high level of human intervention. This was tedious, time intensive, and subject to inconsistent identifications of the cutoffs. For the production of this data set, we developed tools to automatically identify cutoffs and resonances with only minimal guidance from the operator. The increase in efficiency allowed the temporal resolution to be set not by how time intensive the work was, but by how long spectra needed to be averaged to produce a relatively clean spectrum. For this work, we chose to average the spectrum over 1 second intervals. Figure 3 shows diagnostic displays associated with two new analysis tools used to find cutoffs and peaks within spectra. The tools and how they are used are described below.

2.1. Cutoff Detector

[12] Previously, *Ansher et al.* [1992] produced a preliminary electron density data set by identifying the plasma

frequency and therefore the electron density in the Jovian magnetosphere. This data set provided information on sharply defined density structures found in the plasma sheet. *Ansher et al.* [1992] used wideband waveform observations taken from Voyager 1 and 2 that provide high resolution spectra of the nonthermal continuum radiation. The identification process used by *Ansher et al.* [1992] was a manually intensive, subjective technique requiring the operator to manually identify the plasma frequency cutoff from 4-s averaged spectra. *Ansher et al.* [1992] mention the extraordinary time involved with producing such a data set by hand.

[13] Further development of spectral analysis tools has yielded significant success and improvement from the previous method. The present investigation utilizes new software that allows the operator to highlight the general vicinity of the cutoff on a frequency-time spectrogram. Then, an algorithm finds the cutoff in the designated region and records the frequency at 1 second intervals. Hence the automated procedure allows an increase in temporal resolution of a factor of four over the *Ansher et al.* [1992] approach and significantly reduces both manual effort and subjective judgment by the operator.

[14] The cutoff detection algorithm is adjusted by a small number of parameters that can be set by the operator. The first parameter is the cutoff level. In determining possible cutoff candidates, the algorithm scans the region highlighted by the operator and records two separate points, one above the cutoff level and one below. The closer the two points are spectrally, the steeper the slope will be. Therefore the operator can change the location of the cutoff level to manipulate where the algorithm looks for cutoffs within the highlighted region of interest.

[15] The next parameter is the magnitude of the slope which designates the minimum acceptable magnitude of the finite difference slope for the cutoff. The operator may raise the slope magnitude in order to scan only for sharp cutoffs, or lower it in order to accommodate less steep slopes, depending on the quality of the spectrum data.

[16] The cutoff level, slope magnitude and cutoff candidates are displayed by the program for viewing by the operator. When there is more than one possible cutoff, the detection program will display the possible cutoffs. While the algorithm chooses the lowest frequency cutoff by default, the operator may override the algorithm and choose any of the possible cutoffs.

[17] Since the Fourier transform parameters used to produce an individual spectrum yield a spectral resolution of $\sim$28 Hz, this represents the ultimate accuracy with which the cutoff can be determined (with no spectral averaging). Below we discuss consistency checks when two or more characteristic frequencies can be measured and used to determine f_{pe} independently. The different values can then be compared and typically agree to several tens of Hz. Almost all cases agree to within 100 Hz. The uncertainty in f_{pe} translates into a variable uncertainty in the plasma density and is greater in a relative sense when the plasma frequency is low. For example, if we assume an error of 100 Hz in any measurement, a measurement at 300 Hz produces a 70% fractional uncertainty in the density. However, if the measurement is made at 3 kHz, then the fractional uncertainty of the density is much smaller, approximately 7%.

[18] In order to record the confidence of the cutoff frequency measurements, data quality indices were given to each data point. The indices range from 0 to 3 with 0 being a cutoff with the highest confidence and 3 being the least. The amount of noise in the spectrum dictates the quality rating given to a particular data point. Points with a minimal amount of noise are given values of 0, whereas points where the spectral noise is so great that the cutoff is unclear are given a 1 or 2 index depending on the severity of the noise.

[19] A data quality index of 3 is given when there is interference or some other feature in the spectrum making an accurate measurement problematic, or when there is such a significant amount of background spectral noise that the spectra must be time-averaged over a longer period of time in order to interpret the cutoff. For example, the Voyager wideband receivers have notch filters that are used to suppress interference at the power supply frequency of 2.4 kHz and its third harmonic. When a cutoff resides near a notch filter, a data quality index of 3 is used. While the notch filters do not span more than 200 Hz, any measurement made near them is uncertain.

[20] The data quality index allows users to select the confidence level of the data they would like to use. That is, for very accurate measurements an operator can select only high confidence points when using the data, and for a more complete data set where absolute accuracy is less important, one can choose to also include those with poorer quality indices.

2.2. Peak Detector

[21] The program also uses an algorithm for peak detection. Many spectra of interest to this study include Z mode radiation, which has a low-frequency cutoff at $f_{L=0}$. As pointed out by *Barbosa et al.* [1990], the Z mode is often narrowbanded and peaks at this frequency. As the intensity of this peak increases, the width of the emission appears to broaden because of limitations in the Fourier transform and the low dynamic range of the 4-bit waveform system on Voyager. *Barbosa et al.* [1990] demonstrated that taking the peak of the Z mode as $f_{L=0}$ yields the highest consistency in the determination of f_{pe}. Hence when the Z mode is enhanced, we utilize the peak detection algorithm to identify $f_{L=0}$ from which f_{pe} and the electron density can be derived using equation (4). This algorithm can also be used to determine f_{UH} when an enhancement at that frequency is present in the spectrum.

[22] The peak detection algorithm fits a Gaussian curve to the highest peak within the region specified by the program operator. The program then records the frequency of the Gaussian's peak. In order to determine an estimate of the measurement's error, the full-width at half-maximum of the Gaussian curve is measured and recorded along with its peak frequency. The narrower the peak is, the more accurate the measurement will be. This quantitative method is superior to the quality data indices described above. However, to provide a consistent data set we have also translated the width of the peak to quality indices by assigning an index of 0 for $0 < \Delta f \leq 20$ Hz, 1 for $20 < \Delta f \leq 35$ Hz, 2 for $35 < \Delta f \leq 50$ Hz, and 3 for $\Delta f > 50$ Hz.

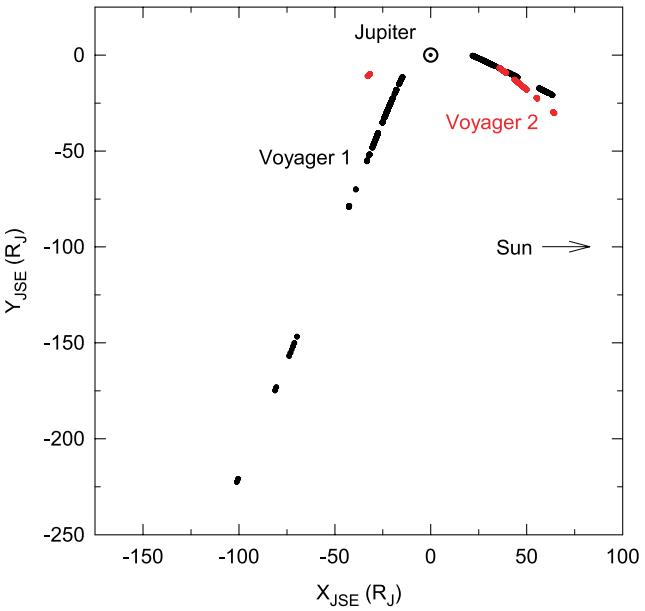

Figure 4. Plot displaying density data coverage for Voyager 1 and 2. Each point represents 1 minute where density was determined in this investigation.

[23] While the operator utilizes a color spectrogram to guide the cutoff and peak detectors, we emphasize that this is only used as a means of identifying the appropriate range in frequency for the algorithm to search. The direct use of color spectrograms tends to mislead an operator to perceive a cutoff that is not equivalent to the cutoff in the actual power spectrum [*Barbosa et al.*, 1990]. Because this may lead to a systematic error, the algorithm utilizes the spectrum itself, and does not depend on a color scale to determine the characteristic frequencies. This should reduce systematic errors and lead to more accurate results.

3. Data Coverage

[24] This data set does not provide complete coverage of the time intervals when the Voyager spacecraft were within Jupiter's magnetosphere. For this data set, two criteria must be met before a determination of the electron density can be made. First, wideband waveform data must exist. These data provide high spectral and temporal resolution measurements of the wave spectrum below 12 kHz but require large telemetry rates in order to return the measurements to the ground. In fact, these data compete with Voyager imaging data for the downlink resource. Hence the data are only available a fraction of the time. When available, they exist in 48-second "frames" which may be continuous, periodic, such as one 48-second frame out of every four such frames, or simply present sporadically. Second, spectral features which exhibit a cutoff or resonance related to the electron density must be present. By far the most prevalent emission of use is the nonthermal continuum radiation. It literally fills the magnetosphere between the magnetopause and higher density regions of the inner magnetosphere. Typically, continuum radiation is not present inside of approximately 20 to 25 Jovian radii R_J. Figure 4 shows the coverage of the density data compiled in this investigation for both Voyager 1 and 2 as projected into the ecliptic plane.

[25] While the present investigation focuses on the outer magnetosphere, the works of *Scarf et al.* [1979] and *Birmingham et al.* [1981] have shown that in the inner magnetosphere, other wave phenomena such as the upper hybrid resonance band can be used to infer the plasma density. For future investigations, the same peak detection tool can be used to accurately determine the plasma density.

[26] The next section discusses in detail the identification of the above mentioned cutoffs and resonances and a consistent set of interpretations of complex spectra, often including Z mode and whistler mode emissions in addition to the continuum radiation.

4. Interpretations of Voyager Plasma Wave Spectra

[27] In order to determine the plasma density from Voyager power spectra, one or more of the characteristic frequencies of the plasma (other than f_{ce}) must be identified from distinguishable spectral features and recorded. Most Voyager plasma wave data exhibit spectra which have one or more visible spectral features (i.e. cutoffs or peaks). In the case where more than one feature is present in the spectrum, we need consistent identifications for the features in order to determine the frequencies of the plasma and to calculate the electron plasma density. We define a consistent interpretation as one where the calculated frequencies (using equations (2) through (5)) are consistent with the spectral features present in the power spectrum. In order to accomplish this, we use a guess-and-check system. The method is as follows:

[28] 1. Assume that one spectral feature present in the spectrum has a cutoff or peak which corresponds to a particular characteristic frequency.

[29] 2. Use the local magnetic field data (which determines f_{ce}) along with equations (2) through (5) to calculate one or more of the other characteristic frequencies.

[30] 3. Look for consistency between the assumed and calculated frequencies and the remaining features present in the spectrum.For example, in a spectrum exhibiting two cutoffs, one might assume the higher frequency feature is f_{pe} while the lower one is $f_{L=0}$. Equation (4) shows the theoretical relation between these two, given f_{ce}. If the measured frequencies do not agree with the theoretical values, then a different pair of cutoffs is assumed, e.g., f_{pe} and $f_{R=0}$. This process continues until the measured cutoffs agree.

[31] Previous studies [*Barbosa et al.*, 1990; *Gurnett and Shaw*, 1973; *Perraut et al.*, 1998] have used similar techniques to arrive at consistent interpretations for Jovian plasma wave spectra. We will now demonstrate our interpretations using examples from Voyager 1 and 2 data used in compiling the new density data set. We will first look at Voyager spectra similar to those addressed in previously published studies (mainly, regions containing one or more spectral features when $f_{pe} > f_{ce}$), and show that our interpretations are consistent with the previous studies. Then, we will examine examples with complex spectra, which few studies have attempted to interpret before, mainly in the lobes where $f_{pe} < f_{ce}$. We will show that it is often possible to find

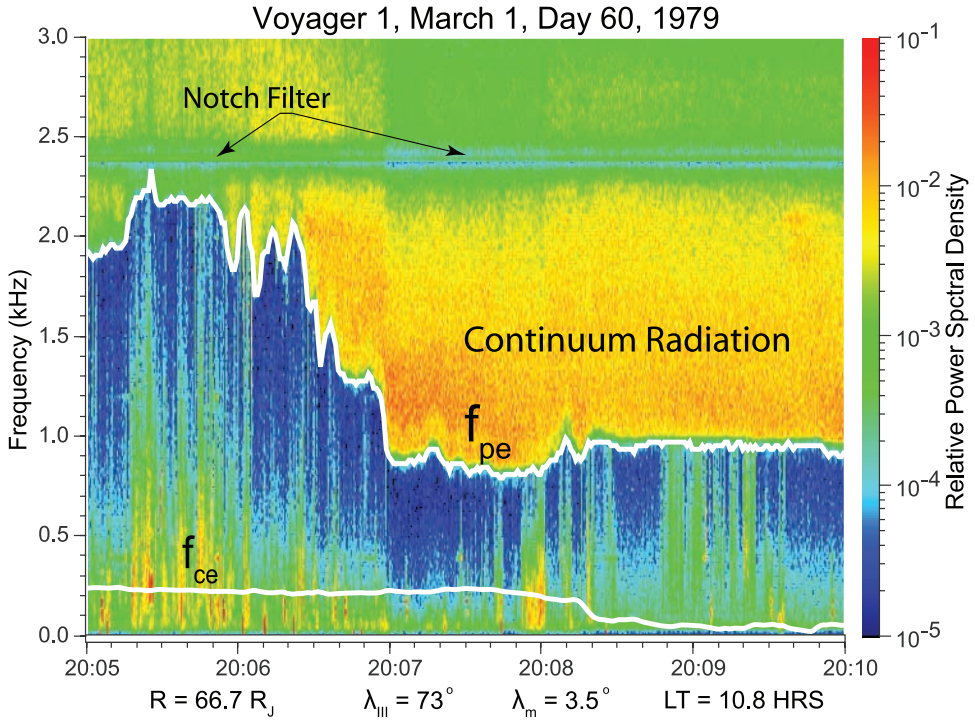

Figure 5. Continuum radiation propagating through the Jovian magnetosphere with a cutoff at f_{pe}. Notice that this is a region wherein $f_{pe} > f_{ce}$. The notch filter, occurring at 2.4 kHz, disrupts cutoff measurements for a brief time near 20:05:25. R is the radial distance from Jupiter in units of Jovian radii R_J, λ_{III} is System III longitude, λ_m is magnetic latitude in degrees (relative to the dipole equator), and LT is the local time in hours.

multiple spectral features which allow an unambiguous identification of the characteristic frequencies, hence, extend the density data set to the low density lobes with some degree of confidence.

4.1. Regions Wherein $f_{pe} > f_{ce}$

4.1.1. Continuum Radiation With One Cutoff

[32] The simplest spectra to interpret for the purposes of determining the electron density are those that include only nonthermal continuum radiation with a single, clear low frequency cutoff and with no other nearby emissions such as the example displayed in Figure 5. For the purposes of this data set, we adopt the *Gurnett et al.* [1981] interpretation that based upon PWS data it is appropriate to assume that the continuum radiation cutoff is the local f_{pe} and using equation (1) we can accurately determine the local electron plasma density. Throughout this paper, the plasma frequency identified in this way will be called the "observed" f_{pe} as opposed to the calculated f_{pe}, which is derived from another spectral feature and using equations (2) through (5). When there is only one cutoff present in the continuum radiation, we have assumed that the continuum radiation is propagating in the ordinary mode and that the cutoff is indeed the plasma frequency. An alternate possibility would be to identify this cutoff as the $R = 0$ cutoff at $f_{R=0}$. However, most theories [*Jones*, 1976; *Shaw and Gurnett*, 1980; *Moses et al.*, 1987; *Barbosa et al.*, 1990] favor the L,O mode as the preferred mode for continuum radiation, hence, we assume that there is always at least some L,O component present when the continuum radiation is detected.

[33] Figure 5 shows Voyager 1 data from 1979 day 060, beginning at 20:05. The plasma frequency is shown as a white trace at the low-frequency cutoff of the continuum radiation. The cutoff detection algorithm has been used to determine f_{pe} and the plasma density is calculated using equation (1). Figure 6 is a plot of the resulting electron density.

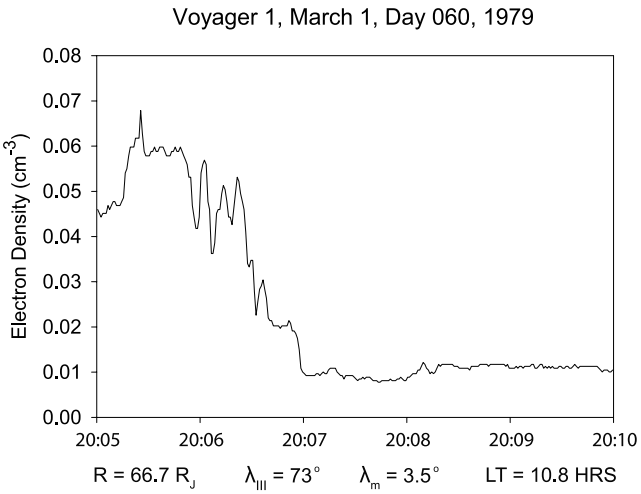

Figure 6. Electron densities determined from the Voyager 1 time period displayed in Figure 5. The density is determined by measuring f_{pe} with the cutoff analysis tool and using equation (1).

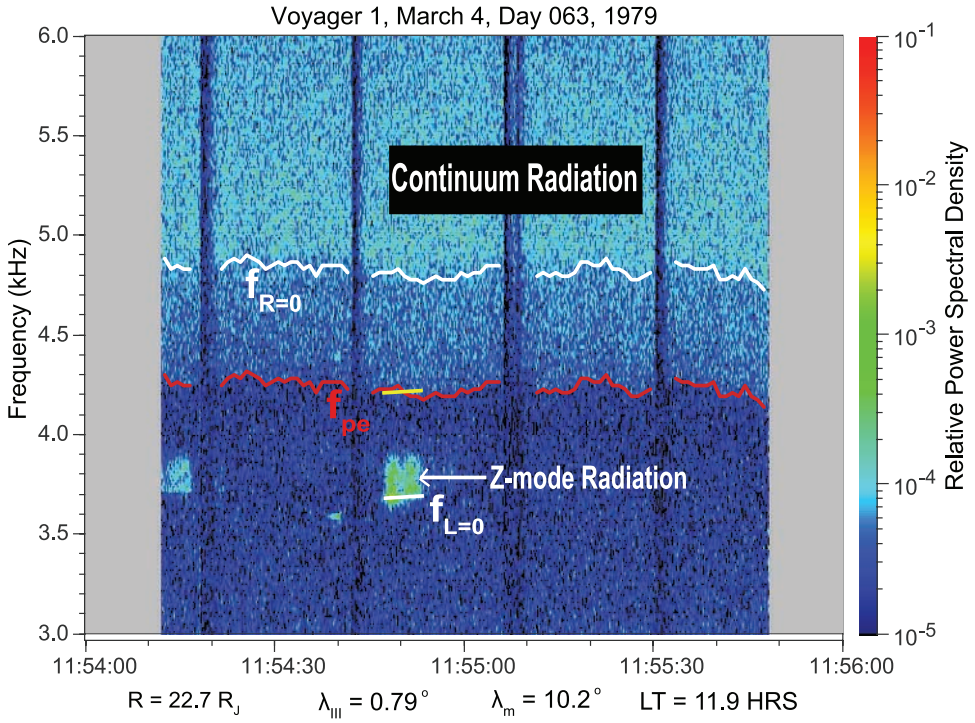

Figure 7. Spectrogram displaying continuum radiation with two cutoffs where $f_{R=0}$ is calculated from the observed f_{pe}. Also, a correct interpretation for f_{pe} calculated from an observed Z mode radiation cutoff at $f_{L=0}$ is demonstrated.

4.1.2. Continuum Radiation With Two Cutoffs

[34] While our data set includes accurate measurements of the observed f_{pe}, and therefore the local electron plasma density, we also found other cutoffs that occur in the data that could be helpful in determining the local electron density. One such situation occurs when two cutoffs are apparent in the continuum radiation spectrum, as shown in Figure 7. On day 063, at 11:54:30, we have identified the low-frequency cutoff as f_{pe} and observe a second cutoff, at somewhat higher frequencies.

[35] The low frequency cutoff is at 4.27 kHz and the higher cutoff is at 4.87 kHz, 600 Hz higher. For this time period f_{ce} is about 1.1 kHz. If we assume the low frequency cutoff to be f_{pe}, and use equations (2) and (3) to calculate $f_{R=0}$, it is apparent that the calculated value of $f_{R=0}$ is approximately 4.8 kHz, very close to the observed upper frequency cutoff. This confirms that the lower frequency cutoff is indeed f_{pe} and the upper frequency cutoff is $f_{R=0}$, the cutoff of the R,X mode. In this example, the continuum radiation is a mix of ordinary and extraordinary modes. This process is reciprocal, meaning that one could, alternately, identify the R,X cutoff and calculate f_{pe}. Either is an equivalent way to determine the plasma frequency. This means that if the R,X cutoff is more clear, it could be used instead of the cutoff at f_{pe}.

[36] The spectrum can become even more complicated when Z mode radiation is present. Next, we will discuss our interpretations for when this emission is present.

4.1.3. Weak Broadband Z Mode Radiation

[37] At 11:54:52 on Day 063, shown in Figure 7, a weak low frequency emission is present below the continuum radiation discussed above. This is characteristic of many of the time periods recorded throughout the Jovian plasma sheet. We first assume that the lower frequency emission is Z mode radiation with a cutoff at $f_{L=0}$. Taking $f_{L=0}$ equal to 3.69 kHz and f_{ce} equal to 1.1 kHz, and using equation (4), we calculate a value for f_{pe} to be 4.20 kHz, which is very close to the observed f_{pe} discussed above. This result is consistent with *Barbosa et al.*'s [1990] interpretation of the cutoff of the broadband Z mode radiation as the $L = 0$ cutoff frequency. Conversely, if f_{pe} is assumed and $f_{L=0}$ is calculated using equation (4) the resulting values for $f_{L=0}$ are very close to the measured cutoff frequency.

[38] Figure 7 demonstrates that f_{pe} calculated from the cutoff of the broadband Z mode radiation is consistent with the observed plasma frequency. Thus it can be inferred that in regions where the plasma frequency is not apparent, for example, where the cutoff at f_{pe} is obscured by Z mode emission, it is possible to use equations (2) and (4) to calculate the plasma frequency from the $L = 0$ cutoff of low intensity broadband Z mode emissions.

4.1.4. Intense Narrowband Z Mode Radiation

[39] Another common occurrence found in both the Voyager 1 and 2 data is an intensification of the narrowband Z mode radiation. *Barbosa et al.* [1990] argued that taking the peak of the narrowband Z mode radiation as $f_{L=0}$ gave the most consistent results. For this investigation we have found our data to be consistent with the interpretation given by *Barbosa et al.* [1990] that where the Z mode is intense and narrowbanded, as opposed to the weak, broadband emission in Figure 7, we assume $f_{L=0}$ is the frequency at the peak of the Z mode.

[40] To demonstrate our agreement with *Barbosa et al.* [1990], we look to another example, shown in Figure 8.

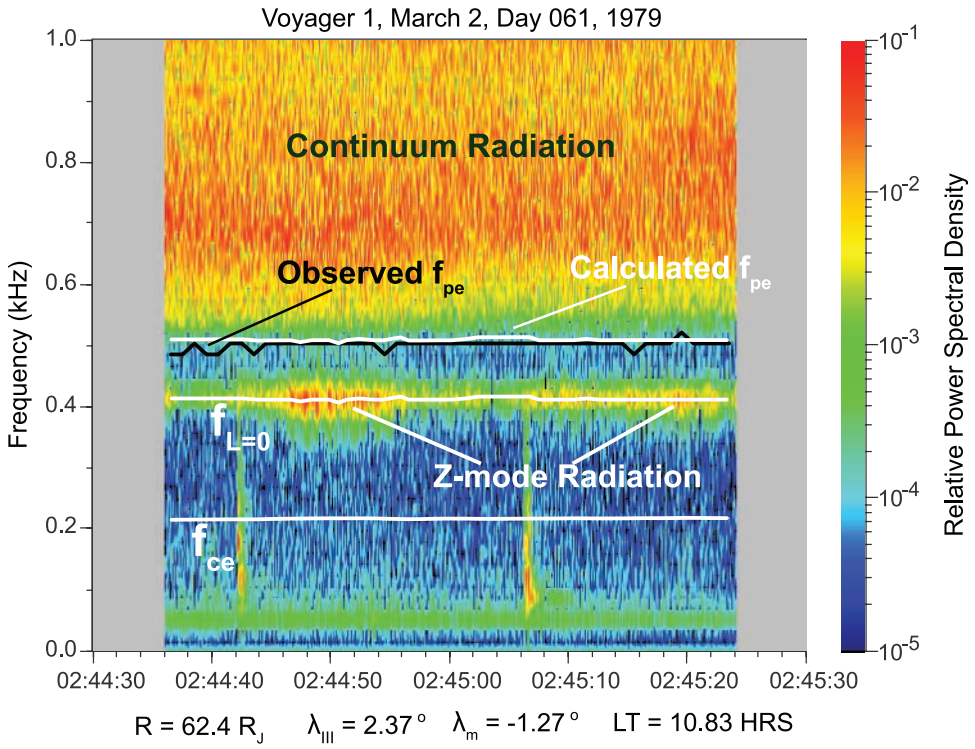

Figure 8. Intense, narrowband Z mode radiation. Interpreting the peak of the Z mode band as the $L = 0$ frequency yields a calculated f_{pe}, which is consistent with the observed f_{pe}.

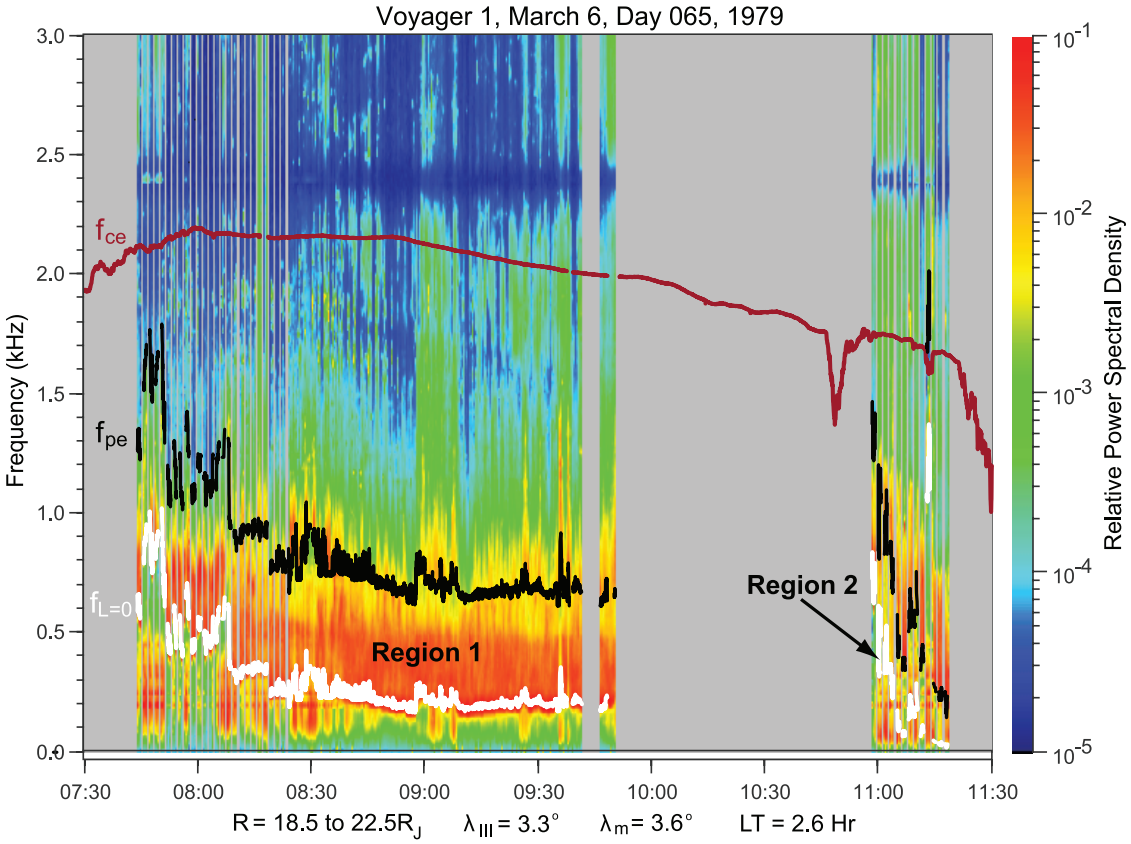

Figure 9. Extended period when $f_{pe} \ll f_{ce}$. The red line denotes the cyclotron frequency. For each region, there is a consistent interpretation for the characteristic frequencies, including f_{pe}. Thus we can determine the plasma frequency in each of these regions.

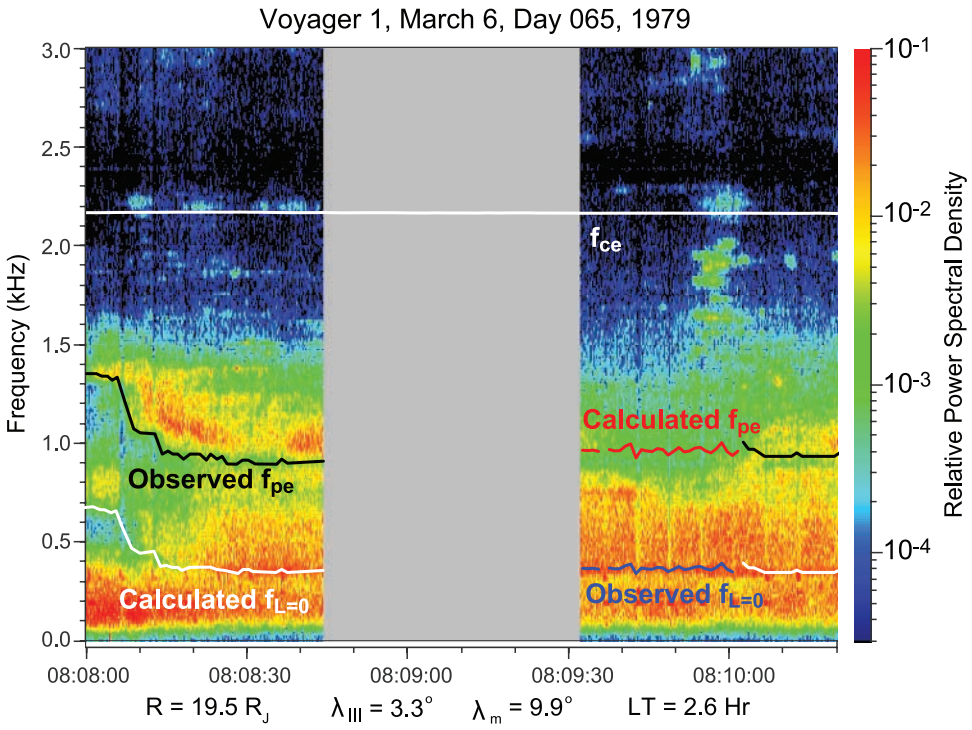

Figure 10. Interpretations of characteristic frequencies by assuming the middle cutoff at 360 Hz to be $f_{L=0}$. Using equations (2) and (4), we calculate f_{pe} and find that it matches the frequency of the higher frequency cutoff quite well. When we assume the middle cutoff is f_{pe}, we find that neither the calculated $f_{R=0}$ nor $f_{L=0}$ match the cutoffs near 86 or 960 Hz.

This is a Voyager 1 example from day 061 in the interval 2:44:30 to 2:45:30 that shows intense narrowband Z mode radiation where the continuum radiation cutoff at f_{pe} is also apparent. Figure 8 uses a white line to identify the peak of the narrowband Z mode radiation which we interpret as $f_{L=0}$. The electron cyclotron frequency is displayed for reference. Notice that the calculated plasma frequency, which was obtained from the observed $f_{L=0}$ and equation (4), is consistent with the observed f_{pe} to within ~20 Hz. Using this interpretation for the L,O mode and calculating the plasma frequency gives results consistent with the cutoff at f_{pe}. Note that, again, this process is entirely reciprocal, meaning either $f_{L=0}$ or f_{pe} can act as the observed frequency and be used with equations (2) and (4) to derive the other frequency.

[41] During some time periods, there is an overlap of continuum radiation and Z mode emissions, obscuring the cutoff at f_{pe} and making it difficult to determine f_{pe} directly. Hence the use of the Z mode cutoff at $f_{L=0}$ extends our ability to accurately determine the local electron density for time periods where the continuum radiation cutoff at f_{pe} is obscured.

4.2. Regions Wherein $f_{pe} \ll f_{ce}$

[42] As Voyager approaches the lobe of the magnetosphere, f_{pe} drops precipitously, often dropping below f_{ce}. *Perraut et al.* [1998] studied such a case obtained by the Galileo plasma wave instrument. Using the Galileo sweep frequency receiver data, they located a region where $f_{pe} \ll f_{ce}$ and provided an identification of the various characteristic frequencies exhibited in the spectrum.

[43] Within the Voyager 1 data set, the most prominent region where $f_{pe} \ll f_{ce}$ occurs on day 065 between 7:00 and 12:00. This is during the outbound pass from a distance of 18.5 R_J to 22.5 R_J. Similar to the example shown by *Perraut et al.* [1998], the spectrum of these regions exhibit three different, but partially overlapping, emissions in the frequency range of 28 Hz to a few kilohertz.

[44] Because the wideband data downlink resource is shared with the Voyager imaging instrument, there are large data gaps within this time period. However, between 07:45 and 10:00 as well as between 11:00 and 11:25, there are high resolution wideband data where $f_{pe} \ll f_{ce}$. Figure 9 displays this entire time period with f_{ce} shown as the red line. Notice that as the density drops, f_{ce} climbs to approximately 2 kHz, much greater than f_{pe}. This occurs as a result of pressure balance. In the plasma sheet, the pressure is dominated by the thermal pressure in the hot plasma sheet particles (high β plasma), while in the lobes the pressure is dominated by magnetic pressure (low β plasma) where

$$\beta = \frac{\mu_0 n k_B T}{B^2} \tag{6}$$

n is number density, k_B is Boltzmann's constant, T is the temperature of the plasma, and B is the magnetic field strength. We will look more closely at two specific regions (labeled 1 and 2 in Figure 9) and determine consistent interpretations for the characteristic frequencies in each region.

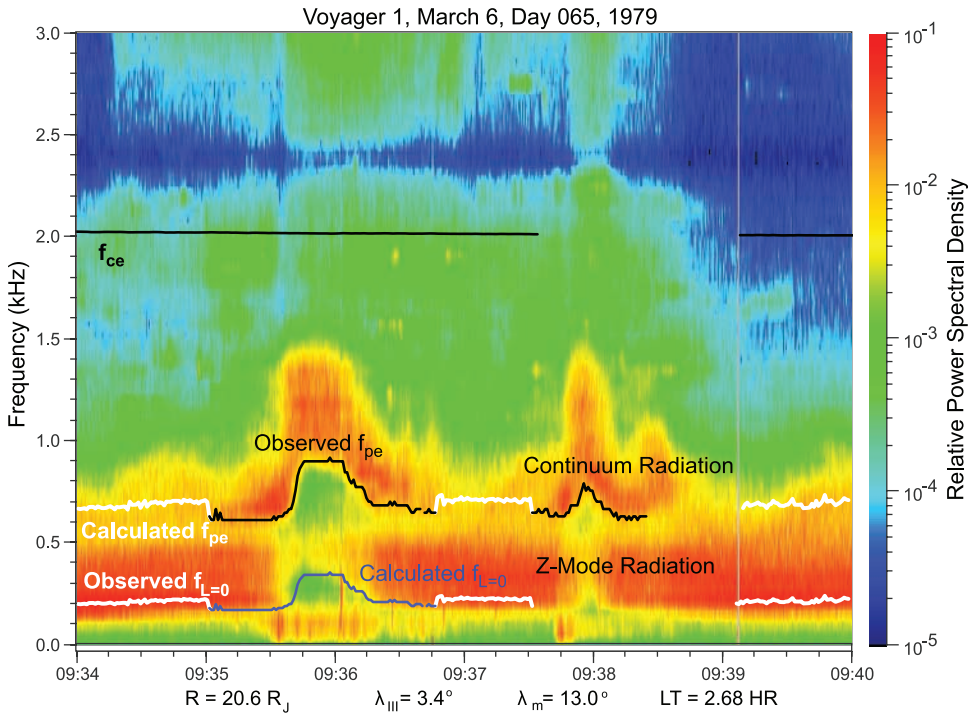

Figure 11. A consistent hypothesis for the interpretation of these three frequency bands in a region 20.6 R_J wherein the $f_{pe} \ll f_{ce}$. The upper band is continuum radiation with a lower cutoff at f_{pe}, the middle band is the Z mode with a lower cutoff at $f_{L=0}$, and the lower band must be the whistler mode.

4.2.1. Cases With Continuum Radiation and Z Mode Radiation

[45] The first region, labeled Region 1 in Figure 9 with detailed views in Figures 10 and 11, exhibits three distinct intense low frequency bands at less than 1.5 kHz. Figure 10 displays a few minutes from day 065 data starting at 08:08:00. The cutoffs are located, from lowest frequency to highest, at approximately 86 Hz, 360 Hz, and 960 Hz. Interpreting the middle frequency as $f_{L=0}$ (white line) and calculating f_{pe} (red line), results in cutoffs that are consistent with the observed cutoffs at 360 and 960 Hz. The wideband receiver has a high-pass filter at 50 Hz; hence, it is likely the cutoff at 86 Hz is instrumental. For the sake of brevity, we present only the interpretation we found to be consistent with the spectrum. If the middle frequency was not assumed to be $f_{L=0}$, but some other frequency, the calculated frequencies would not match the features in the spectrum. Thus we conclude that continuum radiation propagates down to approximately 960 Hz and cuts off at f_{pe}. Below this exists Z mode radiation which cuts off at approximately 360 Hz and whistler mode emissions which extend below $f_{L=0}$. This enables us to accurately determine the density for this region. Also, Figure 9 shows a distinct cutoff located at approximately 300 Hz in Region 1. This cutoff is continuous throughout all of Region 1. We have determined that in Example 1, the cutoff is the $L = 0$ frequency. Now we will look at Example 2, another time period in Region 1, in order to verify this lower frequency cutoff and determine the plasma density for all of Region 1.

[46] Region 1 in Figure 9 with a detailed view in Figure 11 is another example where $f_{pe} \ll f_{ce}$. During this interval, there are two times during which the continuum cutoff is elevated in frequency so that two cutoff frequencies are apparent. We utilize a similar approach as used with Example 1 and postulate that the cutoff of the highest frequency band, at approximately 900 Hz, is f_{pe}. Looking at Figure 11 on day 065 at 09:35:58, it is clear that the calculated value for $f_{L=0}$ (from the measured f_{pe} and equations (2) and (4)) is consistent with the middle cutoff frequency at approximately 350 Hz. We conclude, again, that continuum radiation propagates down to a low frequency cutoff at f_{pe} near 900 Hz, Z mode radiation propagates down to $f_{L=0}$ at approximately 350 Hz, and below this exist whistler mode emissions. The lowest cutoff is likely an instrumental effect caused by the high pass filter at 50 Hz.

[47] A similar example occurs at 09:38, however, a gap in magnetometer data makes the determination of f_{ce} problematic, hence, equations (2) and (4) cannot be applied. However, since f_{ce} is not varying elsewhere in the plotted interval, we can assume f_{ce} is constant. With this assumption it is clear that the cutoffs at f_{ce} and $f_{L=0}$ are similar to those identified in the earlier intervals. Therefore the same interpretation of the wave modes should apply.

[48] The assumption of temporal continuity of the spectra enables the plasma density to be determined for all of Region 1 in Figure 9. When there are two or more cutoffs present in the spectrum we can determine the plasma frequency and the electron density unambiguously and then use these as tie points to connect to times when there is only one cutoff visible in the spectrum. Even though there is only 1 spectral feature (cutoff) during much of the interval plotted in Figure 9, we can rely on the temporal continuity of the spectrum to identify the spectral feature from the tie points. The plasma's density can then be calculated based on the visible cutoff. Specifically, in Region 1, the low frequency cutoff at ~300Hz, is taken as $f_{L=0}$ throughout the

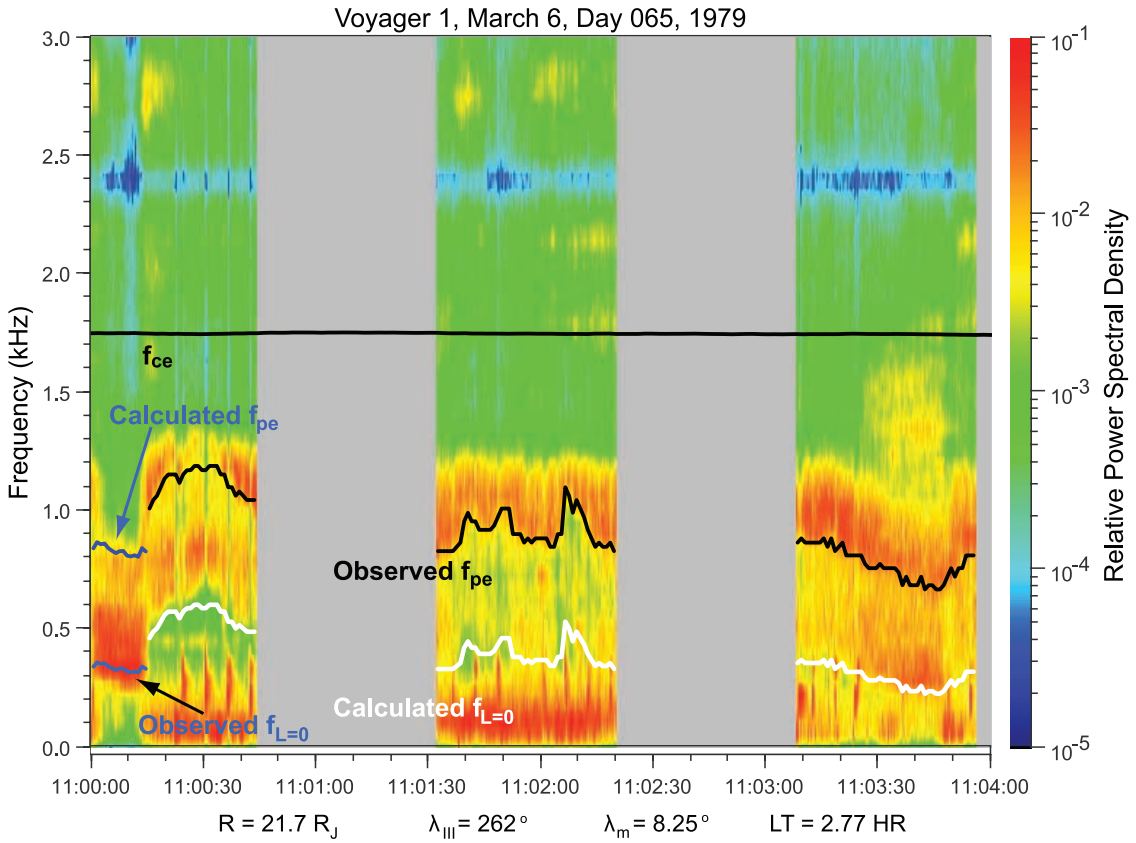

Figure 12. Consistent interpretations between spectral features at f_{pe} and $f_{L=0}$ for a time period during Region 2 (shown in Figure 9). The plasma frequency was measured, and the remaining characteristic frequencies were calculated. This consistent interpretation of the characteristic frequencies of the plasma allow for the density to be determined during this time period.

entire region. Therefore the plasma frequency and density can be calculated even if the plasma frequency cutoff is not visible in the spectrum.

[49] Region 2, shown in Figures 9 and 12, exhibits another region where the plasma frequency is much less than the cyclotron frequency. In this region, the electron cyclotron frequency remains constant at 1.75 kHz. If we postulate that the higher frequency band located at 1.1 kHz at 11:00:30 is the plasma frequency and calculate $f_{L=0}$, the calculated frequency is consistent with the cutoff of the lower frequency band. The same technique was used between 11:01:30 and 11:02:30 and between 11:03:00 to 11:04:00 resulting in the same interpretations. Thus we have consistently interpreted this spectrum and conclude that continuum radiation blends in with the Z mode in much of the interval shown in Figure 9 except for a few times when the density rises such that the cutoff at f_{pe} is clear. Hence the dominant band is Z mode radiation with a cutoff at $f_{L=0}$ that is unambiguously determined in the higher density regions.

4.2.2. Case With Upper Hybrid Resonance

[50] Another example in Region 2 exhibits a serendipitously placed upper hybrid resonance emission occurring at 1.8 kHz from 11:08 to 11:09 and also between 11:11 and 11:12 where f_{ce} is approximately 1.7 kHz, just below the UH bands. This is shown in Figure 13. We assume the spectral peak is f_{UH} and use equations (2), (3), and (5) to calculate both f_{pe} and $f_{L=0}$. At 11:08, if we take f_{UH} to be 1.8 kHz, then the calculated f_{pe} corresponds to the cutoff of the intense emission at approximately 500 Hz. Thus we conclude that the lower frequency emission is a mixture of both Z and whistler modes. A similar example can be found between 11:11 and 11:12. Here the identification of the cutoff near 300 Hz consistently identifies the lower frequency band as the Z mode with $f_{L=0}$ near its peak.

[51] Using the fortunate occurrence of spectra as in Figures 10–13 we were able to unambiguously determine the electron plasma density in Regions 1 and 2. We then assumed continuity of the spectral features to time periods in Figure 9 where there is only one apparent cutoff. Thus we were able to determine the density for a majority of the time in Figure 9. This same technique was used for other regions where $f_{pe} \ll f_{ce}$. *Moses et al.* [1987] and *Perraut et al.* [1998] previously studied low resolution Voyager data and Galileo plasma wave data, respectively, where the $f_{pe} \ll f_{ce}$ and which contained three low frequency bands similar to the high resolution Voyager data in this study. We discuss the consistency of our results with theirs, below.

5. Summary and Discussion

[52] It is of interest to compare the results of this work with those of earlier papers on the interpretation of complex spectra observed when $f_{pe} < f_{ce}$. *Perraut et al.* [1998]

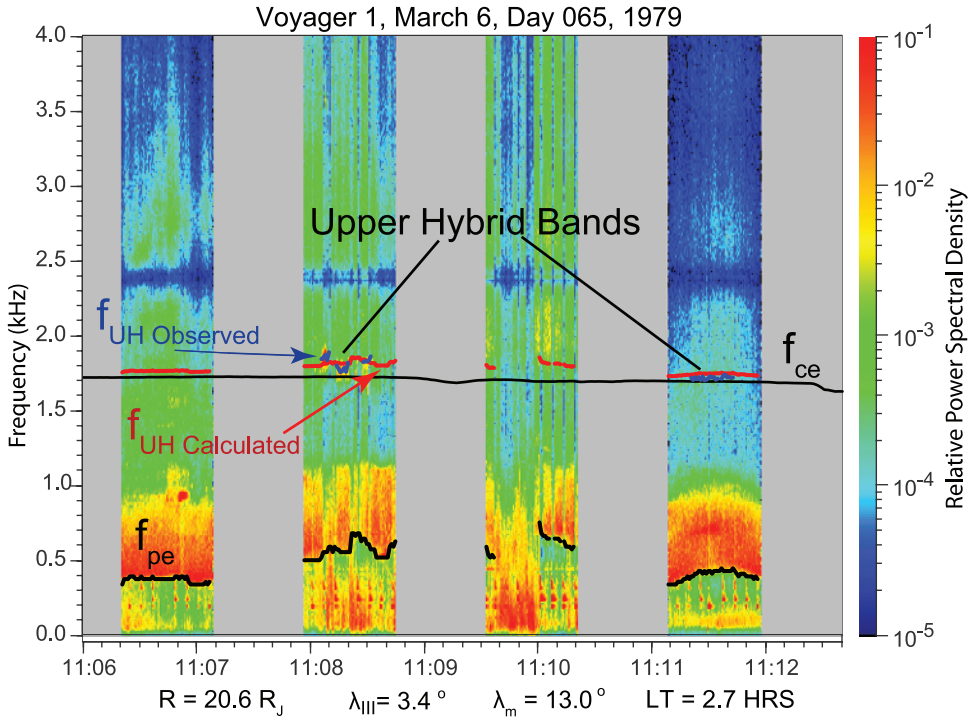

Figure 13. Upper hybrid resonance bands are present along with two unidentified lower frequency bands. Using f_{ce} and equations (4) and (5), we calculate f_{pe} and $f_{L=0}$. The calculated frequencies match features in the power spectrum, giving a consistent interpretation for f_{UH}, f_{pe}, and $f_{L=0}$ when $f_{pe} \ll f_{ce}$.

examined a case which is very similar in many respects to the situation addressed above for the interval covered by Figures 9–13. In fact, these authors used very similar techniques in coming to their conclusions. That is, they looked for two or more cutoffs in the spectrum, hypothesized different identifications for these, and then checked for consistency with the spectral relationships between the various cutoffs using the cold plasma relations used herein. However, at least on the surface, their conclusion for the identification of the mode of the emissions in their example differs from the conclusions arrived at in this paper for obviously different examples. *Perraut et al.* [1998] identified an emission below f_{ce} as ordinary mode emission with a low-frequency cutoff at f_{pe} and employed a second cutoff at $f_{R=0}$ to confirm this. For most of the spectra in Figure 9, we have, conversely, found that the Z mode emission tends to dominate the portion of the spectrum below f_{ce} and that the ordinary mode is usually partially masked by the Z mode. Hence it is usually the case that the most clear cutoff we observe below f_{ce} is that of $f_{L=0}$ instead of f_{pe}. We have used intervals in the observations when a second cutoff was observed to determine that this second, somewhat higher frequency cutoff is f_{pe}, as in Figures 10 through 12. We note that in Figure 13, when narrowband emissions at f_{UH} are observed, the primary cutoff in the spectrum below f_{ce} is, similar to Perraut et al., f_{pe} and that these emissions are ordinary mode.

[53] *Moses et al.* [1987] used a rare rotation of the Voyager spacecraft to measure the polarization of waves at the lowest frequencies in the lobe of the magnetotail. For this example, waves in the frequency range of ~45 Hz to a few hundred Hz showed evidence of waves of "all polarizations" but no electric fields parallel to **B** below this range. Hence they concluded that above 45 Hz, the spectrum includes ordinary mode continuum radiation and that 45 Hz must be f_{pe}. They reported that waves found to have polarizations such that the wave electric field was perpendicular to **B** below 45 Hz could be either Z mode or whistler mode. Since the resonant energy for whistler mode waves would be in the range of 25 MeV, they concluded that the lowest frequency emissions must be Z mode. However, *Perraut et al.* [1998] pointed out that the whistler mode waves needn't be generated locally, hence, the requisite resonant electrons might reside elsewhere. Like *Perraut et al.* [1998], *Moses et al.* [1987] identify the primary mode below f_{ce} as ordinary mode continuum with a low-frequency cutoff defined by f_{pe}. The identification of the lowest frequency band is ambiguous in this case.

[54] The interpretation of the low frequency spectrum in the lobes of Jupiter's magnetosphere below f_{ce} is only possible with sufficient information. When only one cutoff is clearly seen below f_{ce}, the interpretation of that cutoff is likely to be ambiguous. In this paper, as by *Perraut et al.* [1998], the presence of a second cutoff in the spectrum that can be explained by the theoretical relationships between two of the cutoffs and/or resonances defined in equations (1), (3)–(5) can be used to eliminate the ambiguity. Alternately, polarization measurements as in *Moses et al.* [1987] can be used, when available. We have used a method similar to *Perraut et al.* [1998] to make unambiguous identifications of spectral features, when possible. Then, we have assumed that the spectrum evolves in a well-behaved manner to identify otherwise ambiguous cutoffs in adjoining spectra, as in Figure 9. In most cases, we have identified

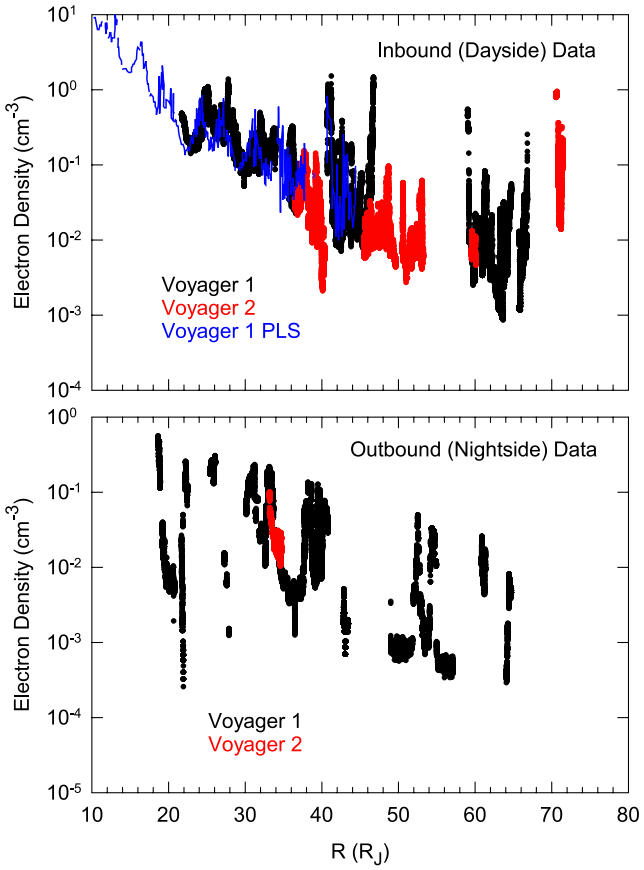

Figure 14. A summary of densities included in the data set. (top) Densities determined by both Voyager 1 (black) and Voyager 2 (red), as well as those measured using the Voyager 1 PLS instrument (blue) during their inbound, dayside trajectories as a function of radial distance from Jupiter. (bottom) Densities from both spacecraft during their outbound, nightside trajectories.

the primary mode below f_{ce} as the Z mode where this can be done unambiguously. It is possible that the spectrum does not evolve smoothly to adjoining regions and that, as in the case of *Perraut et al.* [1998] and *Moses et al.* [1987] this primary mode is actually the ordinary mode bounded at the lowest frequency by f_{pe}. Should this be the case, then our technique would yield a local plasma density that is too high. The cutoff in question is often near a few hundred Hz (see Figure 9) and f_{ce} for these time periods is of order 2 kHz. If we assume the ambiguous cutoff is at 300 Hz and we interpret it by our described process as $f_{L=0}$, the resulting plasma density is of the order of a few times 10^{-2} cm^{-3}. Alternately, if the same cutoff is f_{pe}, then density is of order 10^{-3} cm^{-3}.

[55] The purpose of this investigation is to provide an accurate, high resolution plasma density data set for regions in the Jovian magnetosphere based upon Voyager 1 and 2 plasma wave spectral measurements. Throughout the investigation, it was necessary to employ certain interpretations of the data in order to accurately measure and determine the characteristic frequencies ($f_{UH}, f_{pe}, f_{L=0}, f_{R=0}, f_{ce}$). Using the electron plasma frequency, we were able to accurately compute the local electron density for a substantial amount of time given by the Voyager 1 and 2 plasma wave data. In regions where a clean cutoff at f_{pe} was not apparent, it was necessary to invoke interpretations for other spectral features, including the extraordinary mode and Z mode cutoffs to calculate the local electron density. In regions where both f_{pe} and either the extraordinary mode or Z mode were present, two characteristic frequencies could be used along with the equations of cold plasma theory to validate the mode identifications.

[56] We found that our data was most consistent when we interpreted the cutoff of the nonthermal continuum radiation to be the plasma frequency as described by *Gurnett and Shaw* [1973]. Also, when there is a low intensity broadband emission present, interpreting the low frequency cutoff as $f_{L=0}$ gives a consistent estimate of f_{pe}. However, when there is an intense narrowband Z mode emission present, interpreting the peak frequency as $f_{L=0}$ gives the best estimate of f_{pe}. When two or more characteristic frequencies were present, we checked for consistency between them. In most cases, the agreement was well within 100 Hz. If there were inconsistencies greater than 100 Hz, we deemed our assumptions incorrect. The consistency checks, when possible, led us to conclude that we had made the correct interpretations of the more complex spectra. However, in cases where there existed a mix of continuum radiation, Z mode emissions, and the whistler mode, we verified our interpretation at times when these consistency checks were possible and then interpreted nearby spectra with only one clear cutoff in a self-consistent manner assuming that the spectrum evolved in a continuous manner. We must warn that there is no irrefutable method to verify the interpretation of a single cutoff when multiple wave modes are present.

[57] Figure 14 presents a majority of the density measurements included in the data set. (There are a few brief periods beyond 80 R$_J$ (see Figure 4) that have not been included in this illustration.) For clarity, we have separated the inbound data (taken in the dayside magnetosphere) from the outbound, nightside data. In both panels in Figure 14 there is a general trend for the density to decrease with increasing distance to Jupiter. The dayside data show less variability than the nightside data. The primary exceptions to this are the density peaks (located at approximately 42, 45, 60, 68 and 71 R$_J$) that generally correspond to times when the magnetosphere is compressed and the magnetopause is approaching the spacecraft. The larger variability on the nightside is due to deeper excursions into the lobe, primarily because the Voyager 1 outbound jovigraphic latitude is more extreme ($\sim -6°$) than the inbound ($\sim 3°$). In the upper panel we have reproduced density measurements by *Belcher* [1983] obtained by the Voyager 1 plasma (PLS) instrument. While the data sets do not always include data for the same times, the PLS density trend is clearly in line with those densities included in the present data set. We also note that *Ansher et al.* [1992] made comparisons between PLS densities and those derived from the continuum radiation cutoff in the PWS high resolution data on a much finer timescale and showed similar agreement.

Appendix A: Data Set

[58] Using the methods described above, we examined all of the available Voyager wideband observations for evi-

Table A1. Complete Listing of Columns Provided in the Voyager Density Data Set Compiled and Submitted to the Planetary Data System (PDS)

Column Name	Keyword	Units
SpaceCraft Event Time	SCET	time
Electron Cyclotron Frequency	f_{ce}	Hz
Measured Frequency Value	MEASURED_FREQ_VALUE	Hz
Electron Number Density	n_e	cm^{-3}
Jovigraphic Distance	JOVIGRAPHIC_DISTANCE	Jovian radii
System III Longitude	SYS_III_LONGITUDE	degrees
Magnetic Latitude	MAGNETIC_LATITUDE	degrees
Jovian Solar Ecliptic *X* Coordinate	JSE_X	Jovian radii
Jovian Solar Ecliptic *Y* Coordinate	JSE_Y	Jovian radii
Jovian Solar Ecliptic *Z* Coordinate	JSE_Z	Jovian radii
Magnetic Field Data Present	MAG_CHECK	1 if yes, 0 if no
Data Quality Index	DATA_QUALITY_INDEX	integer, 0–3
Measured Frequency Abbreviation	MEASURED_FREQ_ABBREV	p, R, L, u
Electron Plasma Frequency	PLASMA_FREQ	Hz
$L = 0$ Frequency	L_FREQ	Hz
$R = 0$ Frequency	R_FREQ	Hz
Upper Hybrid Frequency	UH_FREQ	Hz
Full-width at Half-Maximum	FWHM	Hz

dence of spectral features with implications for the electron plasma frequency. Where two or more spectral features were present which allowed for a consistency check, we utilized the feature that was most clearly visible and distinct to determine f_{pe} and the electron density. When only one cutoff was clearly visible we resorted to the continuity reasoning described above to tie to times when an unambiguous determination could be made for the identity of the cutoff. This is really only an issue in the lobes where $f_{pe} < f_{ce}$. The data set, then, is a compilation of the spectral identifications and calculations of f_{pe} (where necessary) and the corresponding electron density.

[59] The final data set has been submitted to the Planetary Data System (PDS) and made available to the scientific community. As described in Table A1, the data set consists of ASCII files with one record per time step. Each record includes the SpaceCraft Event Time (SCET), the electron cyclotron frequency (if available), the frequency of the cutoff or resonance, a code indicating which cutoff or resonance was determined, the calculated electron density, and a set of position coordinates for the spacecraft at the time of the observation. Also included in each record are f_{pe}, $f_{R=0}$, $f_{L=0}$, f_{UH}, full-width at half-maximum measurement and/or the quality index. One of these four frequencies is just a copy of the observed cutoff or resonance frequency. Individual files are used for each day for which there are data. All files are in comma-separated value (CSV) format which enable a user to view them with a standard spreadsheet program.

[60] **Acknowledgments.** This research was supported by NASA grant NNG05GG98G.

[61] Amitava Bhattacharjee thanks the reviewers for their assistance in evaluating this paper.

References

Ansher, J. A., W. S. Kurth, D. A. Gurnett, and C. K. Goertz (1992), High resolution measurements of density structures in the Jovian plasma sheet, *Geophys. Res. Lett.*, *19*, 2281–2284.

Barbosa, D. D., W. S. Kurth, S. L. Moses, and F. L. Scarf (1990), Z mode radiation in Jupiter's magnetosphere: The source of Jovian continuum radiation, *J. Geophys. Res.*, *95*, 8187–8196.

Belcher, J. W. (1983), The low-energy plasma in the Jovian magnetosphere, in *Physics of the Jovian Magnetosphere*, edited by A. J. Dessler, Cambridge Univ. Press, Cambridge, U. K.

Birmingham, T. J., J. K. Alexander, M. D. Desch, R. F. Hubbard, and B. M. Pedersen (1981), Observations of electron gyroharmonic waves and the structure of the Io torus, *J. Geophys. Res.*, *86*, 8497–8507.

Gurnett, D. A. (1975), The earth as a radio source: The nonthermal continuum, *J. Geophys. Res.*, *80*, 2751–2763.

Gurnett, D. A., and A. Bhattacharjee (2005), *Introduction to Plasma Physics: With Space and Laboratory Applications*, Cambridge Univ. Press, Cambridge, U. K.

Gurnett, D. A., and R. R. Shaw (1973), Electromagnetic radiation trapped in the magnetosphere above the plasma frequency, *J. Geophys. Res.*, *78*, 8136–8149.

Gurnett, D. A., W. S. Kurth, and F. L. Scarf (1979), Plasma wave observations near Jupiter: Initial results from Voyager 2, *Science*, *206*, 987–991.

Gurnett, D. A., W. S. Kurth, and F. L. Scarf (1980), The structure of the Jovian magnetotail from plasma wave observations, *Geophys. Res. Lett.*, *7*, 53–56.

Gurnett, D. A., F. L. Scarf, W. S. Kurth, R. R. Shaw, and R. L. Poynter (1981), Determination of Jupiter's electron density profile from plasma wave observations, *J. Geophys. Res.*, *86*, 8199–8212.

Jones, D. (1976), Source of terrestrial nonthermal radiation, *Nature*, *260*, 686–689.

Kennel, C. F., R. F. Chen, S. L. Moses, W. S. Kurth, F. V. Coroniti, F. L. Scarf, and F. F. Chen (1987), Z mode radiation in Jupiter's magnetosphere, *J. Geophys. Res.*, *92*, 9978–9996.

Moses, S. L., W. S. Kurth, C. F. Kennel, F. V. Coroniti, and F. L. Scarf (1987), Polarization of low-frequency electromagnetic radiation in the lobes of Jupiter's magnetotail, *J. Geophys. Res.*, *92*, 4701–4705.

Perraut, S., A. Roux, P. Louarn, D. A. Gurnett, W. S. Kurth, and K. K. Khurana (1998), Mode conversion at the Jovian plasma sheet boundary, *J. Geophys. Res.*, *103*, 14,995–15,000.

Scarf, F. L., and D. A. Gurnett (1977), A plasma wave investigation for the Voyager mission, *Space Sci. Rev.*, *21*, 289–308.

Scarf, F. L., D. A. Gurnett, and W. S. Kurth (1979), Jupiter plasma wave observations: An initial Voyager 1 overview, *Science*, *204*, 991–995.

Shaw, R. R., and D. A. Gurnett (1980), A test of two theories for the low-frequency cutoffs of nonthermal continuum radiation, *J. Geophys. Res.*, *85*, 4571–4576.

Stix, T. H. (1962), *The Theory of Plasma Waves*, McGraw-Hill, New York.

B. L. Barnhart, J. B. Faden, J. B. Groene, D. A. Gurnett, and W. S. Kurth, Department of Physics and Astronomy, University of Iowa, Van Allen Hall, Room 601, Iowa City, IA 52240, USA. (bradley-barnhart@uiowa.edu)

O. Santolik, Faculty of Mathematics and Physics, Charles University, KO Troja, Room A232, V Holesovickach 2, CZ-18000 Praha 8, Czech Republic.